Shallow S wave Velocity Profile from Active Source Seismic Data at the Apollo 14 Landing Site Based on Virtual Multichannel Analysis of Surface Waves

Hikaru Imazato[1], Tatsunori Ikeda[1], and Takeshi Tsuji[2]

[1]Kyushu University
[2]University of Tokyo

July 23, 2023

Shallow *S* wave Velocity Profile from Active Source Seismic Data at the Apollo 14 Landing Site Based on Virtual Multichannel Analysis of Surface Waves

Hikaru Imazato [1], Tatsunori Ikeda [1], Takeshi Tsuji [1,2] *

[1] Department of Earth Resources Engineering, Kyushu University, Fukuoka, Japan

Email: hi.imazato@anawings.co.jp ikeda@mine.kyushu-u.ac.jp

[2] Graduate School of Engineering, The University of Tokyo, Tokyo, Japan

Email: tsuji@sys.t.u-tokyo.ac.jp

Corresponding author: Takeshi Tsuji (tsuji@sys.t.u-tokyo.ac.jp)

7-3-1 Hongo, Bunkyo-ku, Tokyo 113-8656, JAPAN

TEL: +81-3-5841-8684

Email: tsuji@sys.t.u-tokyo.ac.jp

Highlights

- Construct a virtual active-source shot gather using the shots inside two geophones
- Use multichannel analysis of surface waves (MASW) with continuous wavelet transform
- Estimate *S* wave velocity from surface to 10 m depth from noisy data of Apollo 14
- Gradual increase in *S* wave velocity from surface (~50 m/s) to a depth of 6 m (~100 m/s)
- *S* wave velocity deeper than 3 m at the Apollo 14 site is higher than the Apollo 17 site.

Abstract

We used active source seismic data at the Apollo 14 landing site to investigate the shallow *S* wave velocity structure (from the surface to a depth of 10 m) of the Moon. We applied seismic interferometry to data from shots located between two geophones to construct a virtual shot gather for multichannel analysis of surface waves (MASW). We included continuous wavelet transform processing in the MASW analysis to improve the signal-to-noise ratio of the data before estimating the *S* wave velocity V_S profile. The resultant profile showed gradual increase in *S* wave velocity from the surface (V_S =~50 m/s) to a depth of 6 m (V_S =~100 m/s), followed by a harder layer with *S* wave velocity of 110 m/s. This study demonstrated that future extraterrestrial active seismic surveys can be accomplished faster, with simpler field geometry, and using fewer shots and receivers than past missions, thus reducing the payload and cost of future exploration missions.

1 Introduction

Understanding the structure of the shallow lunar subsurface is a prerequisite for future building of bases on the Moon and identifying ice resources to provide water for them. In a recent study, a lunar penetrating radar system aboard a Chinese rover deployed on the far side of the Moon was used to investigate the shallow lunar subsurface structure (Li et al., 2020).

Data from active and passive seismic experiments performed using Apollo Lunar Surface Experiments Packages (ALSEPs; Murtaugh, 2012) deployed during Apollo missions can be used to investigate the structure of the shallow lunar subsurface. The active seismic experiments are more efficient for determining such structure because they are not reliant on the characteristics of ambient noise and can be used to estimate subsurface structures over wider areas of the Moon in a short time. Cooper et al. (1974) used active seismic data recorded during Apollo missions 14, 16, and 17 to identify a low-velocity layer (*P* wave velocity ~100 m/s) extending from the surface to 10 m depth that they interpreted to represent a regolith layer underlain by a layer with a *P* wave velocity of 300 m/s. Tanimoto et al. (2008) applied a cross-correlation approach based on seismic interferometry to ambient noise in Apollo 17 data to

produce an *S* wave structure model from the lunar surface to 15 m depth. Dal Moro (2015) analyzed the Rayleigh-wave group velocity dispersion curve and the horizontal-to-vertical spectral ratio of the active and passive seismic data of the Apollo 14 and 16 missions. However, the validity of the dispersion curve Dal Moro (2015) derived from a single-channel group velocity analysis was compromised by the limited number of available seismic stations and sources (a common problem for analyses of seismic data from Apollo missions).

A promising approach that may improve the stability of *S* wave velocity estimations is to extract dispersion curves by multichannel analysis of surface waves (MASW; Park et al., 1999). However, Apollo mission active seismic data are not suitable for MASW because of the limited number of seismic receivers in the ALSEPs. We therefore investigated the possibility of using seismic interferometry to construct a virtual shot gather to overcome the use of too few geophones and seismic sources during acquisition of the Apollo mission seismic data. Although seismic interferometry analyses usually use only data from seismic sources that lie outside the geophone array, in this study we used virtual seismic sources located between geophones to increase the number of seismograms obtained. By using multiple shots between geophones, MASW is possible with only two geophones. Moreover, because of the poor quality of the active source data, we applied MASW with continuous wavelet transform (CWT; Ikeda & Tsuji, 2019) to enhance surface wave signals. MASW with CWT suppresses noise unrelated to the surface wave signals, thus improving analyses of noisy data and enabling analysis of seismic data recorded with limited numbers of seismometers and seismic sources.

This approach to the use of active seismic data previously recorded by ALSEPs to investigate the shallow lunar subsurface has implications for the design of future seismic surveys on the Moon and Mars.

2 Data

Active seismic experiments (ASEs) were carried out during Apollo missions 14 and 16. In this study, we used the active seismic data recorded using a thumper energy source during the Apollo 14 mission. The ASE data were recorded on 6 February 1971 between 18:09 and 18:37 GMT. Thirteen of 21 thumper shots at 4.572 m intervals were recorded at three geophones at

45.72 m intervals (Figure 1a). Eight shots were unavailable because of either misfires or operational time constraints. The sample interval was 1.887 ms and record lengths were 5 s.

A representative raw data record (Figure 1b) shows signal propagation from shot 17 to the three geophones. The clearest and most stable dispersion curve was derived from the data recorded by geophones 1 and 2 and shots 11, 12, 13, 17, 18, 19, 20, and 21. Conversely, the data recorded by geophone 3 exhibited substantial noise and significantly lower amplitude compared to the others. While we did not discuss the specific sources of noise of the geophone 3, it may be partially due to the wave scattering. Given that our velocity estimation method, as described later, utilizes the initial arrival portions of the direct surface wave, we excluded the data from geophone 3 in our analysis. We used only the data represented by the black symbols in Figure 1a for our *S* wave velocity estimation.

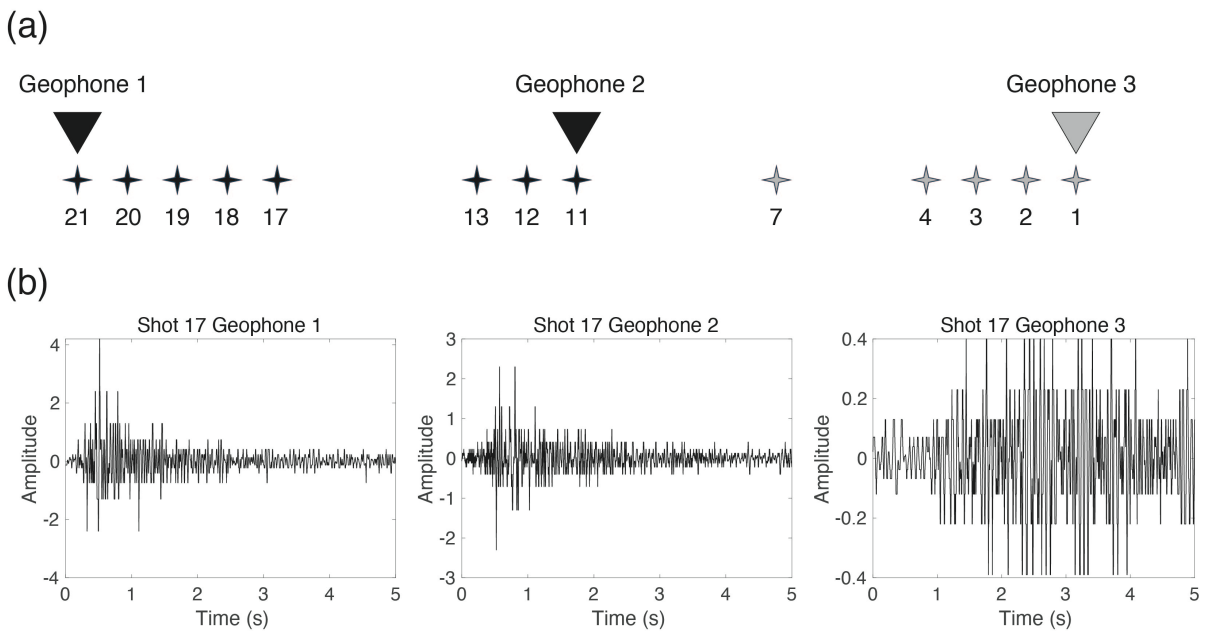

Figure 1. Survey geometry and examples of recorded waveforms. (a) Source–receiver configuration during the thumper source Apollo 14 ASE. Shot numbers are labelled only for the 13 available shots. The ASE data used for MASW analysis in this paper are those from the two geophones and 8 shot locations shown here in black. (b) Raw data from shot 17 as recorded by the three geophones (note different amplitude scales). Because geophone 1 is closer to shot 17 than geophone 2, a stronger first arrival signal arrived earlier at geophone 1. However, geophone 3 includes much noise.

101

102 3 Methods and Results

103 3.1. Construction of Virtual Shot Gathers

104 Constructing shot gathers is an essential step in MASW analysis. Seismic interferometry
105 is a technique that enables the extraction of a Green's function from data recorded at two
106 receivers by means of cross-correlation calculations between the two observation points. This
107 allows for the reconstruction of a single source-receiver data by utilizing the responses of two
108 receivers (Wapenaar, 2004). Because cross-correlation functions can be calculated for each
109 source–receiver pair, a shot gather can be constructed by sorting cross-correlation functions as a
110 function of distance between stations. However, if we were to use only the seismic data from
111 sources that were not located between the two geophones (i.e., geophones 1 and 2) as in the case
112 of Apollo 14 data, there would only be one available geophone interval (Figure 1a) and it would
113 be difficult to obtain shot gather for the MASW analysis. To address this issue, we aim to
114 overcome the limited seismometers and inadequate geometry of sources and receivers for
115 MASW (Figure 2).

116 By assuming a horizontally homogeneous structure beneath the array, we were able to
117 synthesize a virtual shot gather for five geophone intervals by using seismic data whose shots
118 were located between the geophones (Figure 2). First, we moved geophone 1 (located to the left
119 of shot 17 source in Figure 2a) to a virtual location to the right of that source with same distance
120 from shot 17 (i.e., 18.288 m). We then calculated the distance between these two geophone
121 locations (i.e., 9.14 m in Figure 2a), which we defined as the virtual receiver spacing because
122 there was no corresponding spacing in the original data. Then we constructed a virtual shot
123 gather based on that virtual receiver spacing (Figure 2b). Here, we made 2-fold stacks of the
124 waveforms of shots 11 and 21, shots 12 and 20, and shots 13 and 19 in constructing the virtual
125 shot gather, because the virtual receiver spacings for each of these pairs were the same. In
126 computing the cross-correlation functions, receiver stations for virtual sources were defined at
127 the observation point closer to the source. The resulting virtual shot gather calculated from the 8
128 shots and 2 geophones had 5 receiver spacings, which corresponds to a shot gather from one
129 seismic source with 5 geophones (Figure 2b).

We estimated cross-correlation functions by transforming the observed seismic waveforms to the frequency domain and then calculating the complex coherence (e.g., Nakata et al., 2011). To emphasize surface wave signals, we calculated the complex coherence for seismic data for time windows mainly including direct surface waves. The influence of a choice of time windows will be discussed in a later part. The resultant cross-correlation functions for each station with each shot (Figure 3a) show a clear signal from the seismic sources in the 0–1.5 s. Subsequently, we generated a virtual shot gather by considering the receiver spacing, as illustrated in Figure 3b.

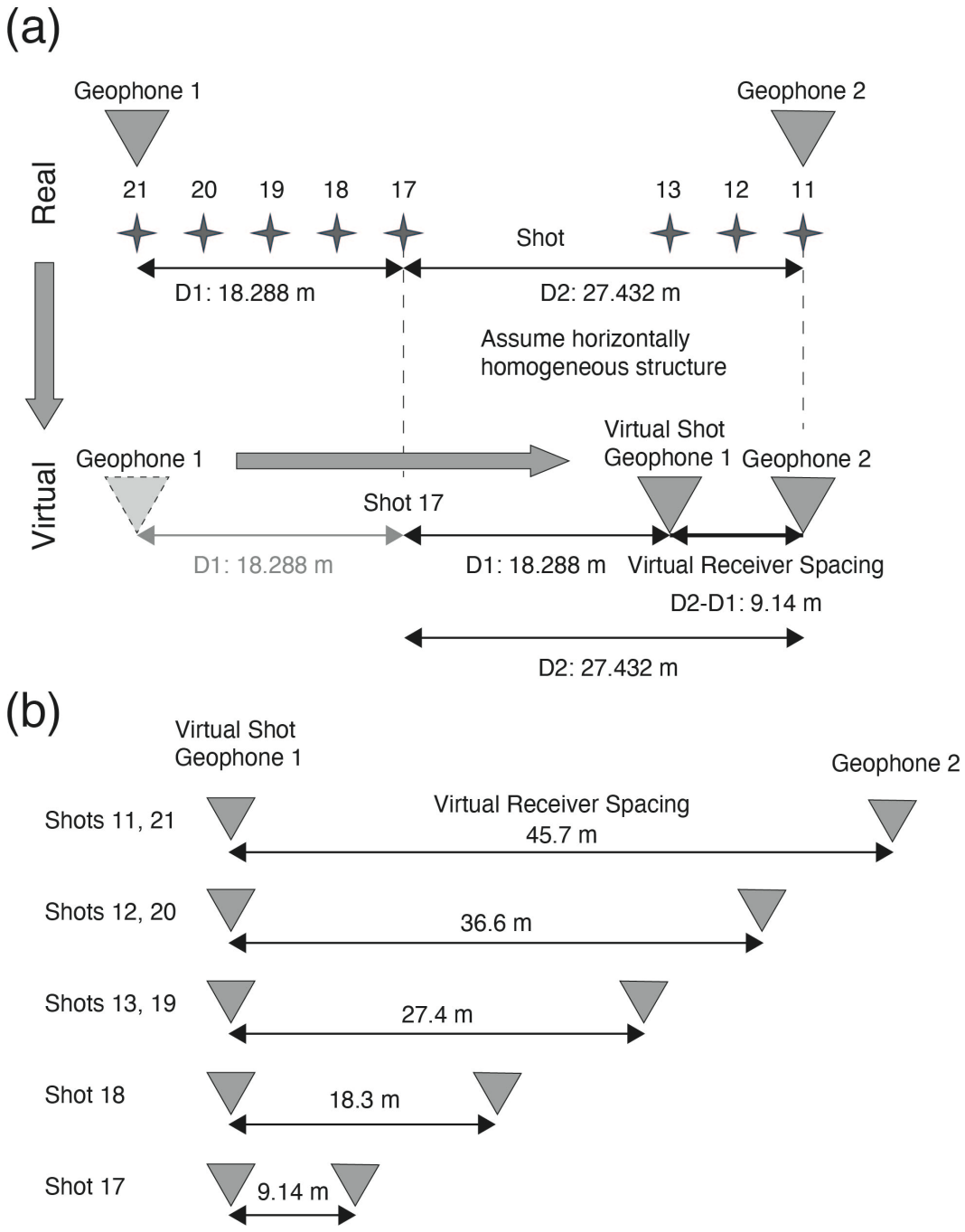

Figure 2. Constructing a virtual shot gather. (a) Original configuration of geophones 1 and 2, and shots 11, 12, 13, 17, 18, 19, 20 and 21. The distances from shot 17 to geophones 1 and 2 are D_1 and D_2, respectively. By relocating both geophones to one side of the shot location, the virtual receiver spacing can be obtained (e.g., $|D_1 - D_2|$ for shot 17). (b) Configuration of all virtual shot gathers.

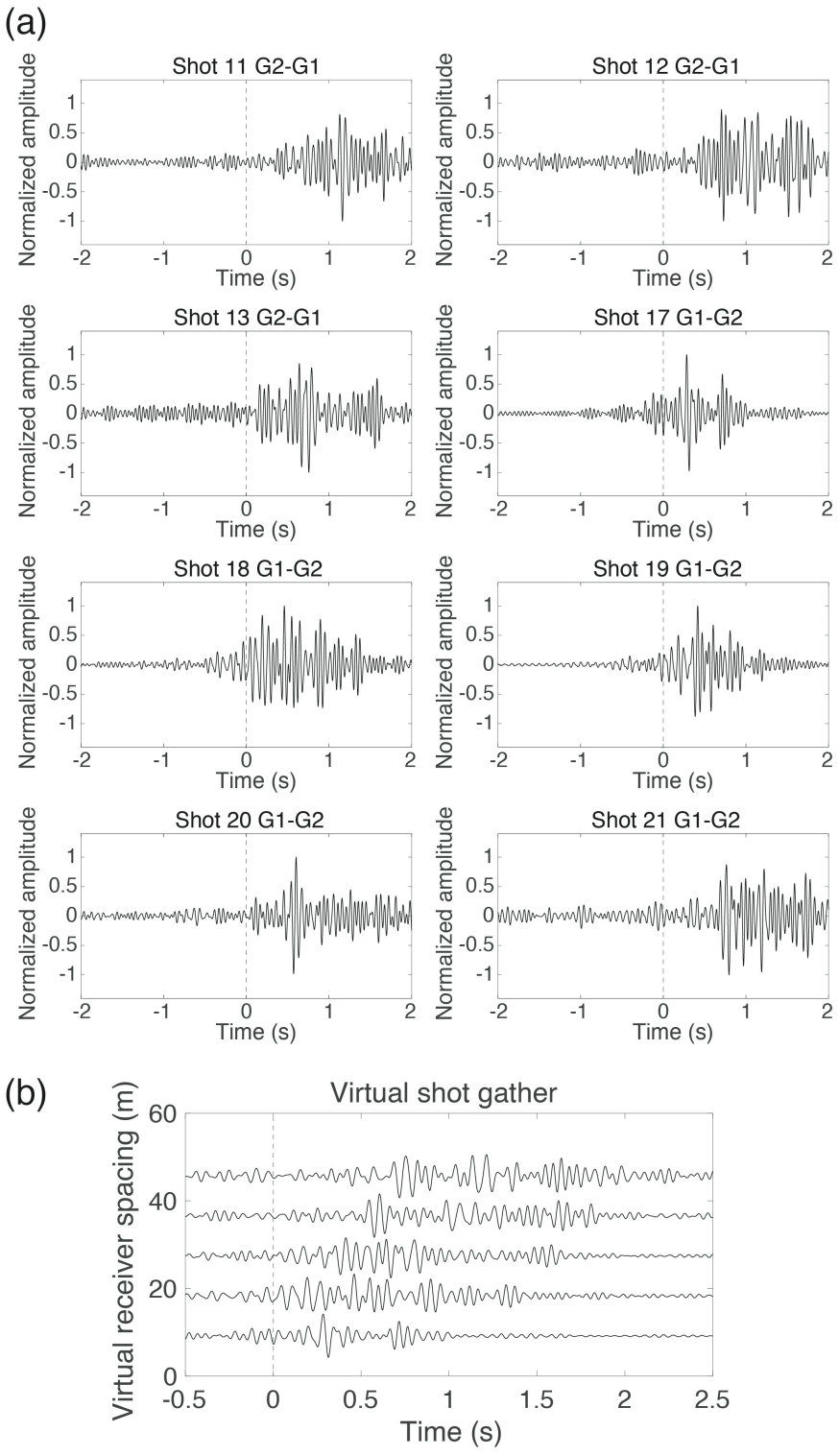

Figure 3. (a) Cross correlations between geophones for each shot. Shot and geophone numbers are shown above each panel. In each analysis, the first geophone number (G1 or G2) corresponds to the virtual source. (b) The virtual shot gather from the Apollo 14 ASE calculated from 8 shots

and 2 geophones. The virtual receiver spacing is the distance between the virtual geophones, calculated from the difference of the distance between the shot and each geophone (see Figure 2b). Each trace represents a cross-correlation function between two stations after 12–22 Hz bandpass filtering. The first arrivals of the signal propagated from the virtual seismic source are observed in the interval 0–1.5 s.

3.2. Calculation of Dispersion Curve from Noisy Data

Surface wave velocity can be approximated by the *S* wave velocity of the interval from the surface to the depth of the wavelength. For Rayleigh wave phase velocity dispersion curves, one-dimensional S-wave velocity profiles can be approximately estimated by plotting S-wave velocity corresponding to 1.1 × phase velocity at depth of the one-third wavelength (e.g., Hayashi, 2008). The phase velocity dispersion curve of the surface wave can be estimated by using MASW to calculate the peak of each frequency from the frequency–phase velocity spectrum (Park et al., 1999). However, the Apollo 14 ASE data are too noisy to allow extraction of clear dispersion images from a virtual shot gather by MASW (see "4 Discussion and Implications"). To reduce the influence of the noise, we estimated the phase velocity dispersion curves by MASW with continuous wavelet transform (CWT; Ikeda & Tsuji, 2019). The MASW with CWT method first estimates group velocity from the time when the waveform amplitude of a shot gather is at its maximum. Then it estimates the phase velocity from the phase of the group wave arrival time (Ikeda & Tsuji, 2019). Because this analysis focuses on phase around the dominant group wave arrival time, it helps to suppress any noise that is unrelated to the signal of the surface waves. The MASW with CWT method of Ikeda and Tsuji (2019) can be summarized as follows.

The stacked cross coherence CC_{AB} between the data recorded by receivers *A* and *B* at receiver spacing d_j for the *j*th receiver pair (i.e., the virtual shot gather in this study) is described by the equation

$$CC_{AB}(f, d_j) = exp\left(-i\frac{2\pi f}{c(f)}d_j\right), \quad (1)$$

where f is the frequency and c is the phase velocity.

Based on the wavelet propagator derived by Kulesh et al. (2005) and Holschneider et al. (2005), Ikeda and Tsuji (2018) presented the relation of the wavelet transform of cross-coherence W as

$$W_{CC_{AB}}(t,f,d_j) = exp\left(-i2\pi f d_j\left(\frac{1}{c}-\frac{1}{u}\right)\right) W_s\left(t-\frac{d_j}{u},f\right), \quad (2)$$

where t is time, $W_{CC_{AB}}(t,f,d_j)$ is the wavelet transform of cross coherence for the jth receiver pair, u is the group velocity, and W_s is the wavelet transform of 1 in the frequency domain. We used the Morlet wavelet as the mother wavelet.

To distinguish surface wave signals from noise, we calculated the arrival times of dominant group waves. We computed amplitude spectra in the frequency–group-velocity domain as

$$U(u,f) = \sum_j \left|W_{CC_{obs}}(u,f,d_j)\right|, \quad (3)$$

where $u\ (= d_j/t)$ is the group velocity, and $W_{CC_{obs}}$ is the wavelet transform of the observed shot gather. The group velocity at each frequency is defined as the group velocity with maximum amplitude in the amplitude spectra U.

Then, we estimated the phase velocity dispersion curve by using phase information corresponding to the arrival times of estimated group waves. We computed amplitude spectra in the frequency–phase-velocity domain by using the wavelet propagator of equation (2) and the group velocity dispersion curve of equation (3) as

$$C(c,f) = \left|\sum_j \frac{W_{CC_{obs}}(t_u,f,d_j)}{\left|W_{CC_{obs}}(t_u,f,d_j)\right|}\frac{\overline{W_{CC_{AB}}(t_u,c,f,d_j)}}{\left|W_{CC_{AB}}(t_u,c,f,d_j)\right|}\right|, \quad (4)$$

where the overbar signifies a complex conjugate and t_u is the arrival time of group waves. We calculated the phase velocity at each frequency with maximum C in equation (4). However, the phase velocity dispersion curve for inversion was determined by picking continuous phase velocities with local maximum C in equation (4).

The estimated group velocity dispersion curve obtained by MASW with CWT (Figure 4a) is clearly observed at 7–15 Hz and corresponds to velocities of about 37–41 m/s. The phase velocity dispersion curve (Figure 4b) appears at 7–15 Hz and corresponds to velocities of about 50–70 m/s. To estimate *S* wave velocity models to satisfy estimated group and phase velocity dispersion curves (blue lines in Figures 4a and 4b), we used both group and phase velocities for inversion of *S* wave velocity.

3.3. *S* Wave Velocity Structure

By applying surface wave inversion to the estimated dispersion curves, we constructed a 1D layered *S* wave velocity structure by using an iterative least-squares inversion based on algorithms in Computer Programs in Seismology (CPS) by Herrmann (2013). The initial model was a stepped gradient based on the work of Tanimoto et al. (2008) as follows. Ten horizontal layers, each 1 m thick, were constructed. Density at the surface was set at 1800 kg/m^3 and *P* and *S* wave velocities at 80 and 40 m/s, respectively (blue line in Figure 4d). At 10 m depth, density was set at 1933 kg/m^3, and *P* and *S* wave velocities at 193 and 97 m/s, respectively. The velocities and densities for each layer were based on linear interpolations between 0 and 10 m depth with the interpolated values at the midpoint of each layer applied to the whole of that layer. In the inversion, we searched the *S* wave velocity of each layer. The P wave velocity of each layer was estimated from the S wave velocity assuming the Poisson's ratio is constant (0.33 in our study). The density of each layer was fixed for the initial model during inversion.

The good agreement between the observed dispersion curve of phase and group velocities and the ones obtained from the inverted S-wave velocity structure (Figure 4c) indicates a satisfactory inversion. The inverted *S* wave velocity model (red line in Figure 4d) shows a gradual increase in *S* wave velocities down to a depth of 6 m (~100 m/s). To assess the depth resolution of our inversion, we computed the depth sensitivity of fundamental mode Rayleigh waves of phase and group velocity for *S* wave velocity (CPS; Herrmann, 2013) (Figure 5a). Our analysis indicates high sensitivity at depths of 1–3 m within the frequency band used for inversion (6.9–15 Hz), which then decreases with depth. For lower frequencies, the analysis showed the sensitivity of our inverted results to be reasonable to a depth of 7 m.

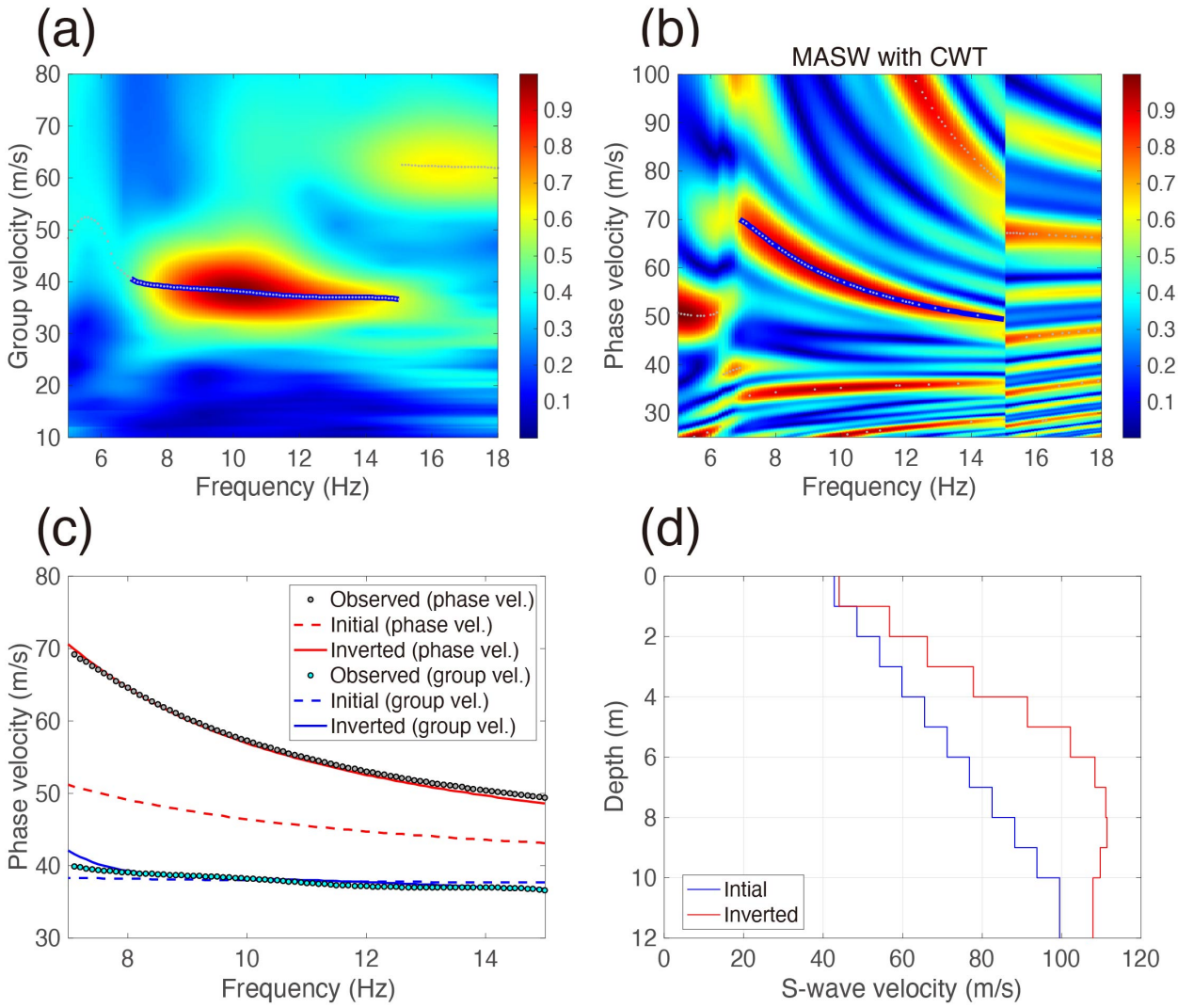

Figure 4. Dispersion curves of (a) group velocity and (b) phase velocity calculated by MASW with CWT. In panel (a) hotter colors represent larger values of $U(u,f)$ in equation (3), and in panel (b) they represent larger values of $C(c,f)$ in equation (4). The color scale is normalized by the maximum value. The gray dots in panels (a) and (b) are the maximum velocities at each frequency of the spectrum. The blue lines are the picked dispersion curves for inversion. (c) Theoretical and observed phase and group velocity dispersion curves. The dashed lines are the theoretical dispersion curve calculated from the initial model (blue line in panel d), the solid lines are the theoretical curve for the inverted model, and the green line is the phase velocity estimated by MASW with CWT. (d) Comparison of the inverted *S* wave velocity structure (red line) and the initial stepped gradient model (blue line). Note that the inverted *S* wave velocity structure is final model in this study.

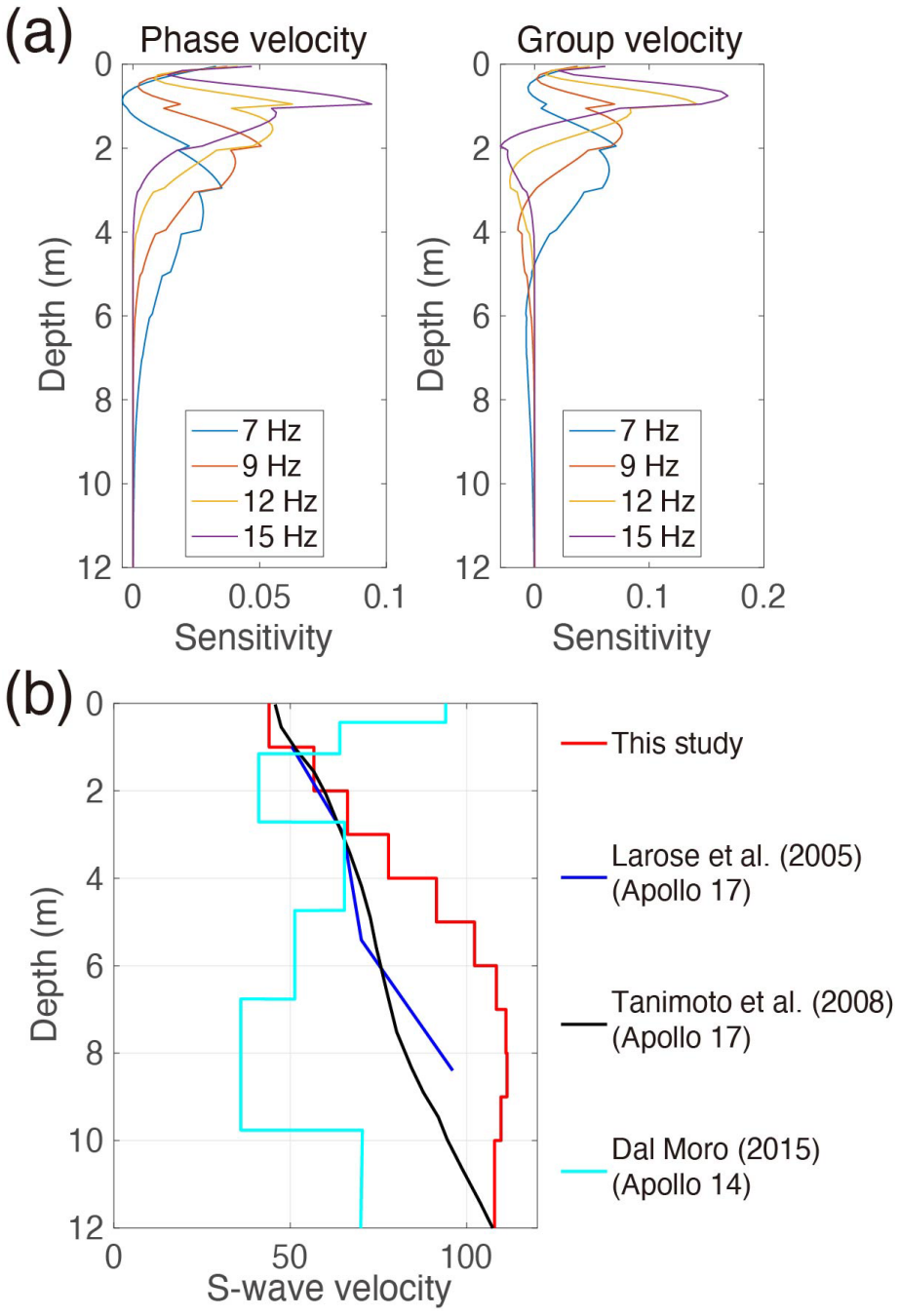

Figure 5. (a) Depth sensitivity kernels of fundamental mode Rayleigh waves of phase and group velocities for *S* waves at frequencies 7, 9, 12, and 15 Hz. We use phase and group velocities in the frequency range 6.9–15 Hz for our inversion. (b). Comparison of the inverted *S* wave velocity models (red line) with the previous models by Larose et al. (2005) using Apollo 17 data, Tanimoto et al. (2008) using Apollo 17 data, and Dal Moro (2015) using Apollo 14 data.

4 Discussion and Implications

As we described, the virtual shot gathers were calculated from seismic data for the time window mainly including direct surface waves. Specifically, we defined the time window corresponding to velocity from 20 to 200 m/s. One may consider using later arrival times would be suitable because cross correlation of the coda part may make it possible to retrieve the Green's function between stations due to large scattering of seismic waves on the Moon.

To investigate the influence of a choice of the time window, we compared virtual shot gathers and resulting dispersion images including the case with the conventional MASW without CWT for different time windows (Figure 6). We compared three cases: (1) whole 5 sec time window, (2) earlier time window corresponding to arrival times of wave velocities from 20 to 200 m/s, and (3) later time window corresponding to arrival times of wave velocities from 40 m/s to 5 sec. The results show when using the earlier time window, direct surface waves are clearly observed in the virtual shot gather (Figure 6b). The phase velocity dispersion images derived from the conventional MASW without CWT do not show clear signals when using the whole latter time windows (Figures 6j and l). However, applying MASW with CWT extracts clear phase velocity dispersion images from noisy shot gathers (Figures 6g and i), indicating the robustness of MASW with CWT for noisy data. On the other hand, using the earlier time window, dispersion signals are observed in the phase velocity dispersion image without CWT (Figure 6k), although the fluctuation is suppressed with CWT (Figure 6h). Therefore, we analyzed seismic data for the earlier time window in this study.

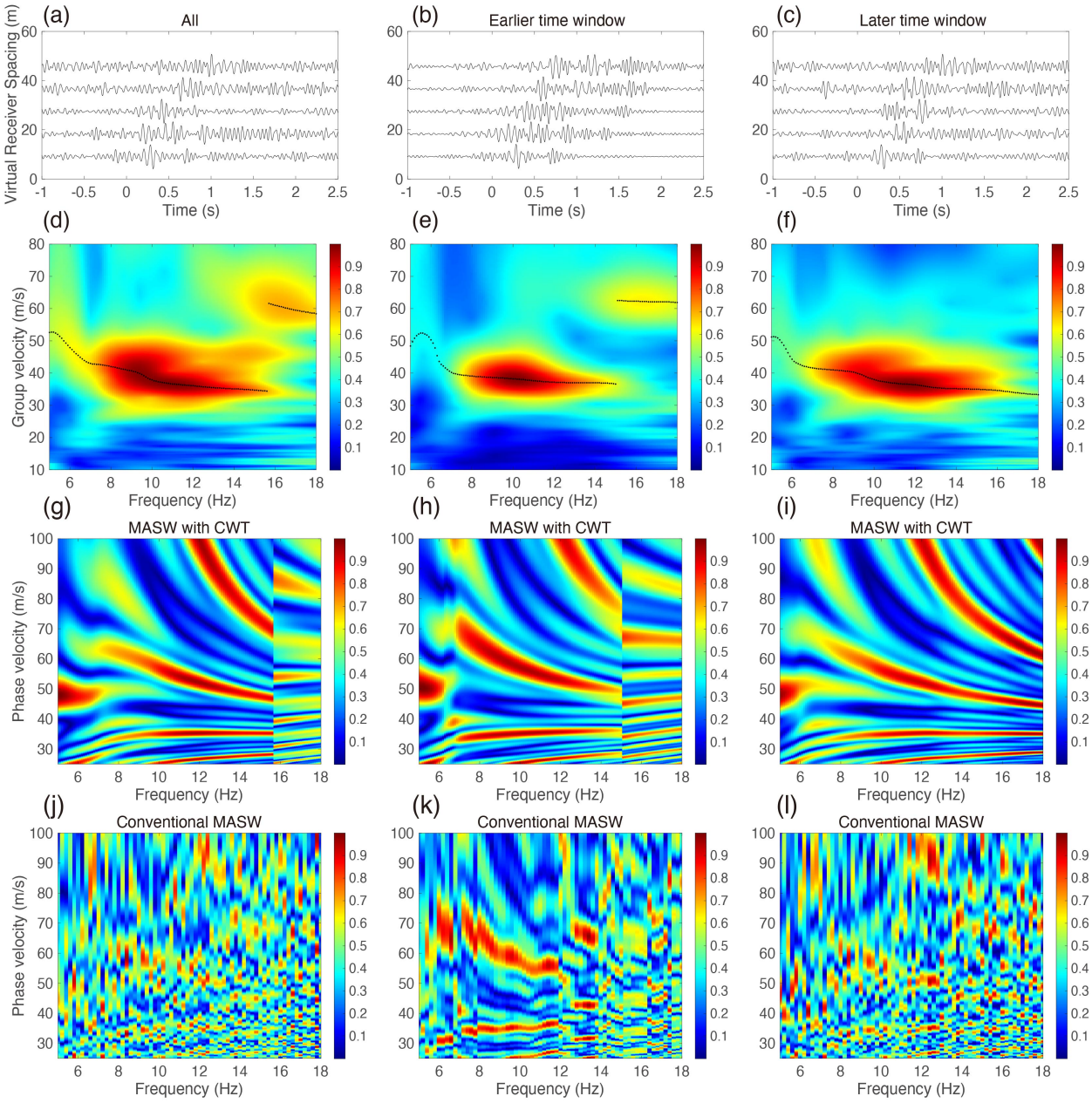

Figure 6. Comparison of virtual shot gathers and dispersion images when using different time windows. (a, b, and c) virtual shot gathers (d, e, and f) group velocity dispersion images, (g, h and i) phase velocity dispersion images by MASW with CWT, and (j, k, and l) phase velocity dispersion images by the conventional MASW when using whole time window, earlier time window, and later time window, respectively. The black dots in panels (d), (e), and (f) are the maximum coherence at each frequency of the spectrum.

Our virtual multichannel analysis of surface waves from Apollo 14 ASE data showed that gradual increase in *S* wave velocity from the lunar surface (~50 m/s) to a depth of 6 m (~100 m/s). Below this surface layer, we identified a harder layer with *S* wave velocity of 110 m/s. Here we compare the results of the *S* wave velocity structure of the shallow lunar subsurface at the Apollo 14 landing site with those of previous research. Cooper et al. (1974) identified a regolith layer extending from the surface to a depth of about 10 m at the Apollo 14, 16, and 17 landing sites by seismic refraction analysis. This velocity structure aligns with our *S* wave velocity structure (Figures 4d, 5b). However, our *S* wave velocity structure (red line in Figure 5b) differs from that of Dal Moro (2015), who analyzed the same Apollo14 data (light blue line in Figure 5b). There are several potential reasons for this discrepancy. First, Dal Moro (2015) used both joint inversion of the group velocity dispersion from the Apollo 14 dataset and the horizontal-to-vertical spectral ratio, whereas we used phase velocity dispersion curves derived from 8 shots and 2 geophones. Second, Dal Moro (2015) used a higher frequency dispersion curve than that of our study, considering higher modes of surface waves and horizontal to vertical spectral ratio.

To evaluate the variations in shallow geological structures, we compared our results with seismic velocity models obtained from a different landing site (Apollo 17). The shallower sections of our *S* wave velocity profile (0-3 m depth) are similar to those of Larose et al. (2005) (blue line in Figure 5b) and Tanimoto et al. (2008) (black line in Figure 5b), both of whom analyzed Apollo 17 data. Larose et al. (2005) and Tanimoto et al. (2008) analyzed group velocity dispersion curves in the frequency range from 4 to 10 Hz and 5 to 9 Hz, respectively, while we analyzed group and phase velocity dispersion curves in the frequency range from 6.9 to 15 Hz. Therefore, our investigation depth is shifted to the shallower part. These three models should be sensitive to S-wave velocity at ~3 m depth, and this similarity indicates that the lunar surface layer (<3 m depth) at the Apollo 14 and 17 landing sites have similar characteristics. However, at deeper than 3 m depth, our *S* wave velocity at the Apollo 14 site is higher than that observed at the Apollo 17 site.

In comparison to the passive approaches employed by Larose et al. (2005) and Tanimoto et al. (2008), our active source-based approach offers a notable advantage in terms of data recording time efficiency. We used ASE data that took less than 30 minutes for recording, while Larose et al. (2005) and Tanimoto et al. (2008) used passive seismic data that required a

longer recording time. Although our approach necessitates the preparation of an active seismic source, the utilization of a minimal seismic source with minimal energy consumption could prove valuable for lunar or Martian exploration. For instance, a portable active seismic source (PASS) capable of generating a broad frequency signal (Tsuji et al., 2023a) has been recently designed for the purpose of exploring the Moon. Despite its small size (a 4 cm diameter motor), the PASS achieved signal propagation up to 1 km for horizontal distance on Earth by stacking repeated seismic source signals. Utilizing such a minimal seismic source, along with a limited number of seismometers, enables the imaging of the subsurface structure of the Moon (see Figure 8 in Tsuji et al., 2023b).

By using ASE data (i.e., active seismic data with limited numbers of receivers and active sources), we successfully obtained a reliable *S* wave velocity profile within a short timeframe and without having to rely on unpredictable ambient noise data. Moreover, our approach using MASW with CWT effectively handled noisy data. Our results demonstrate that shallow seismic surveys in extraterrestrial environments can be carried out more effectively (faster, more flexibly, and therefore at lower cost) using less equipment and simpler source–receiver geometry than in the past, thereby reducing the payload necessary for future extraterrestrial exploration missions.

Acknowledgments

We thank the Data ARchives and Transmission System (DARTS) for providing seismic data acquired by Apollo mission. We also thank to Taichi Kawamura (IPGP) for fruitful discussion. This study was supported through the Japan Society for the Promotion of Science (KAKENHI grant JP20H01997; JP21H05202; JP22H05108; JP20K04133) and the Institute of Space and Astronautical Science/JAXA.

Data and Resources

We used data obtained from the DARTS provided by the Center for Science-satellite Operation and Data Archive (C-SODA) at Institute of Space and Astronautical Science (ISAS) / Japan Aerospace Exploration Agency (JAXA). The seismic data is available from the following URL. https://www.darts.isas.jaxa.jp/planet/seismology/apollo/ASE.html

References

Li C., Su, Y., Pettinelli, E., Xing, S., Ding, C., Liu, J. et al. (2020). The Moon's farside shallow subsurface structure unveiled by Chang'E-4 Lunar Penetrating Radar. *Science Advances*, 6(9). https://doi.org/10.1126/sciadv.aay6898

Cooper, M.R., Kovach, R.L., Watkins, J.S. (1974). Lunar near-surface structure. *Reviews of Geophysics*, 12(3), 291–308. https://doi.org/10.1029/RG012i003p00291

Dal Moro, G. (2015). Joint analysis of Rayleigh-wave dispersion and HVSR of lunar seismic data from the Apollo 14 and 16 sites. *Icarus*, 254, 338–349. http://dx.doi.org/10.1016/j.icarus.2015.03.017

Hayashi, K. (2008). Development of Surface-wave Methods and Its Application to Site Investigations (Ph.D. Dissertation). Kyoto University.

Herrmann, R.B. (2013). Computer Programs in Seismology: An Evolving Tool for Instruction and Research: *Seismological Research Letters*, 84(6), 1081-1088. https://doi.org/10.1785/0220110096

Holschneider, M., Diallo, M.S., Kulesh, M., Ohrnberger, M., Lück, E., Scherbaum, F. (2005). Characterization of dispersive surface waves using continuous wavelet transforms. *Geophysical Journal International*, *163*(2), 463–478.

Ikeda, T., and Tsuji, T. (2018). Surface-wave tomography for near-surface characterization with continuous-wavelet transform for two-station crosscorrelation: SEG Technical Program Expanded Abstracts 2018, 2531‑2535.

Ikeda, T., and Tsuji, T. (2019). Multichannel analysis of surface waves with continuous wavelet transform for near surface applications: Fifth International Conference on Engineering Geophysics, Al Ain, UAE, 21-24 October 2019. https://library.seg.org/doi/10.1190/iceg2019

Ikeda, T., and Tsuji, T. (2020). Two-station continuous wavelet transform cross-coherence analysis for surface-wave tomography using active-source seismic data. *Geophysics*, *85*(1), EN17–EN28.

Kulesh, M., Holschneider, M., Diallo, M.S., Xie, Q., Scherbaum, F. (2005). Modeling of Wave Dispersion Using Continuous Wavelet Transforms. *Pure and Applied Geophysics*, *162*(5), 843–855.

Larose, E., Khan, A., Nakamura, Y., Campillo, M. (2005). Lunar subsurface investigated from correlation of seismic noise, *Geophysical Research Letters*, 32. doi:10.1029/2005GL023518

Murtaugh, C.R., (2012). Apollo lunar surface experiments package: *Aerospace Research Central*. https:/doi.org/10.2514/6.1966-919

Nakata, N., Snieder, R., Tsuji, T., Larner, K., Matsuoka, T. (2011). Shear wave imaging from traffic noise using seismic interferometry by cross-coherence. *Geophysics*, *76*(6), SA97–SA106.

Park, C.B., Miller, R.D., Xia, J. (1999). Multichannel analysis of surface waves: *Geophysics*, 64, 800–808.

Tanimoto, T., Eitzel, M., Yano, T. (2008). The noise cross-correlation approach for Apollo 17 LSPE data: Diurnal change in seismic parameters in shallow lunar crust: *Journal of Geophysical Research*, 113, E08011. doi:10.1029/2007JE003016.

Tsuji, T., Tsuji, S., Kinoshita, J., Ikeda, T., Ahmad, A.B. (2023a). 4 cm portable active seismic source (PASS) for meter- to kilometer-scale imaging and monitoring of subsurface structures, Seismological Research Letters, 94(1), 149-158, doi:10.1785/0220220049.

Tsuji, T., Kobayashi, T., Kinoshita, J., Ikeda, T., Uchigaki, T., Nagata, Y., Kawamura, T., Ogawa, K., Tanaka, S., Araya, A. (2023b). Lunar active seismic profiler for investigating shallow substrates of the Moon and other extraterrestrial environments, Icarus, 404, 115666, doi:10.1016/j.icarus.2023.115666.

Wapenaar, K. (2004). Retrieving the elastodynamic Green's dfunction of an arbitorary inhomogeneous medium by cross correlation, Physical Review Letters, 93, 254301.